High elemental selectivity to Sn submonolayers embedded in Al using positron annihilation spectroscopy

C. Hugenschmidt,* P. Pikart, M. Stadlbauer, and K. Schreckenbach
Physics Department E 21 and FRM II, Technical University Munich, 85747 Garching, Germany
(Received 14 January 2008; published 26 March 2008)

In the present work, we demonstrate that metal layers in the submonolayer range embedded in a matrix are revealed with unprecedented sensitivity by coincident Doppler-broadening spectroscopy of the positron annihilation using a monoenergetic positron beam. The measured electron momentum distribution specific for Sn is clearly observable in Al/Sn/Al-layered samples even at a Sn area density of as low as 7.3×10^{-2} μg/cm^2 below 200 nm Al. An explanation for the high elemental selectivity for the thin Sn layers is set forward in terms of efficient positron trapping due to the changing positron affinity at the Al/Sn-interface and quantum-dot-like positron states in Sn nanoparticles.

DOI: 10.1103/PhysRevB.77.092105 PACS number(s): 73.21.Ac, 78.70.Bj

I. INTRODUCTION

When a positron is implanted in a material, it thermalizes rapidly (approximately picoseconds), diffuses through the crystal lattice (~100 nm), and finally annihilates as a delocalized positron from the Bloch state or from a localized state present in open-volume defects. The positron-electron annihilation in matter is completely dominated by the emission of two 511 keV photons in opposite directions in the center-of-mass system. In the laboratory system, the transversal momentum of the electron p_T—the momentum of the fully thermalized positron is negligible—leads to a deviation of the 180° angular correlation of the annihilation radiation. The longitudinal projection of the electron momentum onto the direction of the γ-ray emission p_L results in a Doppler shift of the 511 keV γ quanta by $\Delta E = \pm \frac{1}{2} p_L c$ (see, e.g., in reviews on positron physics).[1,2]

For this reason, the detection of the Doppler broadened 511 keV annihilation line enables a nondestructive examination of the electron momentum distribution at the positron annihilation site. The annihilation of conduction electrons in metals leads typically to a small Doppler shift $\Delta E < 2$ keV, whereas the large binding energy of core electrons results in a ΔE of several keV. Therefore, the events with high Doppler shift, i.e., in the outer tail of the 511 keV photoline, correspond to the annihilation of inner shell electrons and contain hence information of the chemical surrounding at the annihilation site.

In coincident Doppler-broadening spectroscopy (CDBS), both annihilation quanta are detected in coincidence with two high-resolution Ge detectors, which leads to an efficient background suppression by several orders of magnitude in order to reveal the unique element specific signature in the tail of the 511 keV photoline.[3] A number of experiments were carried out on pure metals and semiconductors in order to detect the element specific signature in the 511 keV annihilation line.[4–9] The influence of the crystal structure and lattice defects on the measured electron momentum distribution was studied in detail by Alatalo *et al.*[10] Nagai and coworkers applied CDBS in order to study the chemical surrounding of defects and precipitation aging in metallic alloys.[7,11–13] In more recent coincident Doppler-broadening (CDB) investigations, the chemical surrounding at the annihilation site was examined in several binary and ternary alloys.[14–18]

In contrast to previous CDB studies, the investigation of layered samples requires a mono-energetic positron beam, which allows the adjustment of the appropriate positron implantation depth. In the present work, thin Sn layers embedded in Al have been investigated by CDBS. Besides the application of a nondestructive technique, one aim has been to reveal the elemental signature of Sn of various thicknesses in the CDB spectra in order to investigate the positron trapping properties of the embedded Sn layer.

II. EXPERIMENT

A. Sample preparation

For the presented experiment, a set of four Al/Sn/Al-layered samples was prepared in an UHV chamber using 0.5 mm thick glass substrates. The thickness of the thinnest Sn layer embedded in an Al matrix was as small as 0.1 nm. First, pure Al ($\geqslant$99.99%) with a thickness of 5.5 ± 0.3 μm was evaporated onto the water-cooled glass substrate in order to exclude that even 15 keV positrons with a mean penetration depth of 1.1 μm would reach the glass. Afterwards, the Sn layer ($\geqslant$99.999%) of various thicknesses d_{Sn} (d_{Sn}=0.10 ± 0.03, 1.60 ± 0.1, 25 ± 1, and 200 ± 8 nm) was evaporated on top of the Al. Finally, the Sn layer was coated by 200 ± 8 nm Al. The accuracy of the layer thickness is related to the evaporation time and the precision of the evaporation rate measured by a piezothickness monitor (0.01 nm/s). In addition, annealed Al and annealed Sn serve as reference materials.

B. Calculation of the positron implantation profile

We performed calculations of the Makhovian implantation profile of the layered samples in order to maximize the overlap of the positron distribution with the Sn layer by variation of the kinetic energy of the positrons. The simulated implantation profile prior to positron diffusion or trapping is exemplarily plotted in Fig. 3(a) for 6 keV positrons in a 25 nm Sn layer below 200 nm Al. A high fraction of positrons is stopped in the Sn layer (denoted by f) due to the high stopping power of Sn. As a result of these calculations, the kinetic energy was set to 6 keV for the three samples, with Sn thicknesses of 0.10, 1.6, and 25 nm, respectively, and to 15 keV for the others. The material dependent parameters for the calculation are listed for Al and several other elements in the publication by Puska and Nieminen[19] and references therein. The values for Sn are not reported so far and were therefore approximated via an interpolation of known parameters, which lead to an accuracy of 11%–17% of the calculated f. In addition, the results of these simulations confirm that even at a kinetic energy of 15 keV, no positron would reach the glass substrate below the Al/Sn/Al layers.

A calculation of the positron annihilation sites cannot be performed reliably, since it requires structure information of the embedded Sn layer, material dependent diffusion constants, and in particular preassumptions about the trapping rates at the Sn/Al interface. However, the distribution of accumulated annihilation events including diffusion and trapping can be approximated at least qualitatively: In this simple model, isotropic diffusion in Al after implantation (diffusion length of 140 nm and typical positron lifetime of 200 ps) and trapping at the Al/Sn interface or in the Sn layer are assumed, i.e., positrons implanted in the Sn layer would not escape into the Al matrix. Taking into account the positron annihilation rate during diffusion in Al, the amount of positrons diffusing from Al to the Al/Sn interface was calculated and added to the number of positrons implanted in Sn in order to get an estimate of positrons annihilating in the Sn layer. The resulting distribution of positron annihilation sites is shown in Fig. 3(b).

C. Coincident Doppler-broadening spectrometer

The measurements were carried out with the CDB spectrometer[18] located at the high intensity positron source NEPOMUC—neutron induced positron source Munich.[20] The positron intensity at the sample position was 2×10^6 moderated positrons per second and the beam diameter amounted to 2 mm. The electronic stability and the energy resolution were monitored by recording the 477.6 keV γ line of ^{7}Be during the measurement. Albeit at the high single count rate of $\sim2\times10^4$ counts/s, no considerable deterioration of the energy resolution of $\Delta E=1.38$ keV at $E=477.6$ keV is observed due to the use of digital signal processing modules (Canberra) for the electronic data acquisition.[21] The overall momentum resolution of the CDB measurement was $\Delta p_L\approx4.3\times10^{-3}m_0c$. The measurement time was set to 10 h per spectrum resulting in typically 1.1×10^7 counts in the coincidence spectrum of the 511 keV photopeak.

III. MEASUREMENTS AND RESULTS

The raw data of the CDB spectra are normalized to the same integrated intensity of the 511 keV photopeak and are plotted in Fig. 1. Note the low background leading to a peak-to-background ratio of better than 10^5. The inset shows the photon intensity in the high-momentum region for $p_L\geqslant10\times10^{-3}m_0c$ significantly above the Fermi momentum of Al, $p_F=6.77\times10^{-3}m_0c$. The higher photon intensity for larger electron momenta with increasing amounts of Sn is attributed to the higher binding energy of the annihilating core electrons in Sn.

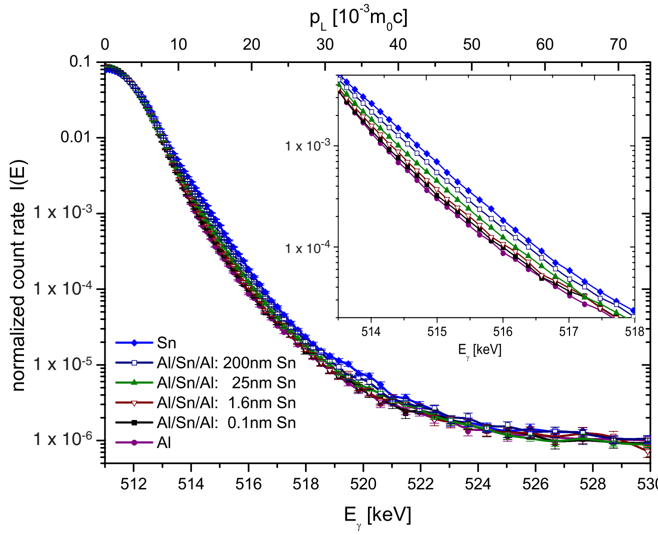

FIG. 1. (Color online) CDBS of the 511 keV annihilation line profiles for pure Al, Sn, and the Al/Sn/Al layered samples with various Sn thicknesses (normalized to the same intensity). The inset shows a zoom into the high-momentum region and highlights the differences between the samples.

For a more detailed view, all spectra have been divided by the spectrum, obtained for pure annealed Al, in order to reveal the element specific contribution of Sn (Fig. 2). Even at an amount of 0.1 nm Sn below the 200 nm Al coating, the photon intensity increases significantly for $10\times10^{-3}m_0c<p_L<25\times10^{-3}m_0c$. The higher photon intensity in the high-momentum region due to the appearance of the Sn signature corresponds to positrons, which annihilate with core electrons of the Sn atoms. With increasing Sn thickness, the signature of Sn emerges more and more clearly and approaches the curve obtained for pure Sn. The solid lines represent least-squares fits of a linear combination of the photon intensities recorded for pure Sn $I_{\mathrm{Sn}}(E)$ and pure Al $I_{\mathrm{Al}}(E)$. The fit function $I_{fit}=(1-\eta)I_{\mathrm{Al}}(E)+\eta I_{\mathrm{Sn}}(E)$ has only one free fit parameter η, which corresponds to the amount of positrons annihilating in the Sn layer and can be regarded as an amplitude of the observed Sn signature (see Table I). Consequently, the fraction $1-\eta$ corresponds to positrons, which annihilate in the Al bulk or from a surface state after back diffusion, where the amount of positrons close to the surface is small [see Fig. 3(b)]. The fitting procedure was applied for Doppler shifts greater than 2.5 keV in order to avoid distortions due to the annihilation of conduction electrons. Therefore, the plotted I_{fit} curve agrees very well with the data for high momenta, but it is not a good approximation in the low-momentum region below $p_L\approx7\times10^{-3}m_0c$.

Table I shows the obtained values for the layered Al/Sn/Al samples with various Sn thickness d_{Sn}. The reference samples of pure Al and pure Sn are listed as well. The

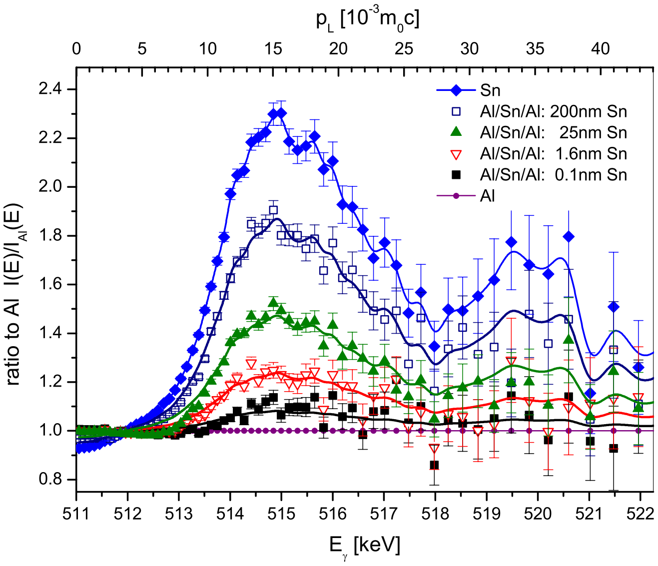

FIG. 2. (Color online) Ratio curves of the Doppler broadened 511 keV line depicted in Fig. 1. All spectra are divided by the reference spectrum obtained for pure annealed Al. The uppermost curve shows the elemental signature of Sn. Even at an amount of 0.1 nm, the signature of Sn emerges clearly. The data of the layered samples were fit by a linear combination of the photon intensities recorded for Sn and Al (solid lines).

fit parameter η corresponds to the measured amount of positrons, which annihilate in the Sn. The higher values of η, in particular, at low Sn content highlight the extreme sensitivity of CDBS with monoenergetic positrons to the embedded Sn layer in Al that is attributed to efficient positron trapping at the Sn. This effect is visualized qualitatively by the distribution of the positron annihilation sites including diffusion and trapping in Sn [see Fig. 3(b)]. Thus, the experimentally determined amount of positrons, which annihilate at Sn atoms after diffusion and trapping η, is larger than the calculated amount of positrons, which have been implanted in the Sn layer f.

IV. DISCUSSION

The strongly disproportional increase of the positron annihilation rate with core electrons from Sn is interpreted as follows: After implantation, thermalized positrons diffuse to

TABLE I. Results for the layered samples. d_{Sn}: Sn thickness below the 200 nm Al coating; f: calculated fraction of positrons implanted in the Sn layer; η: observed fraction of positron annihilation in Sn. Pure Al and Sn serve as references.

Sample	d_{Sn} (nm)	d_{Sn} ($\frac{\mu g}{cm^2}$)	f	η
Al	0	0	0	0
$Al/Sn_{0.1}/Al$	0.1	0.073	7.49×10^{-4}	0.063
$Al/Sn_{1.6}/Al$	1.6	1.166	1.19×10^{-2}	0.183
$Al/Sn_{25}/Al$	25	18.23	0.170	0.364
$Al/Sn_{200}/Al$	200	145.8	0.304	0.670
Sn	⋯	⋯	1	1

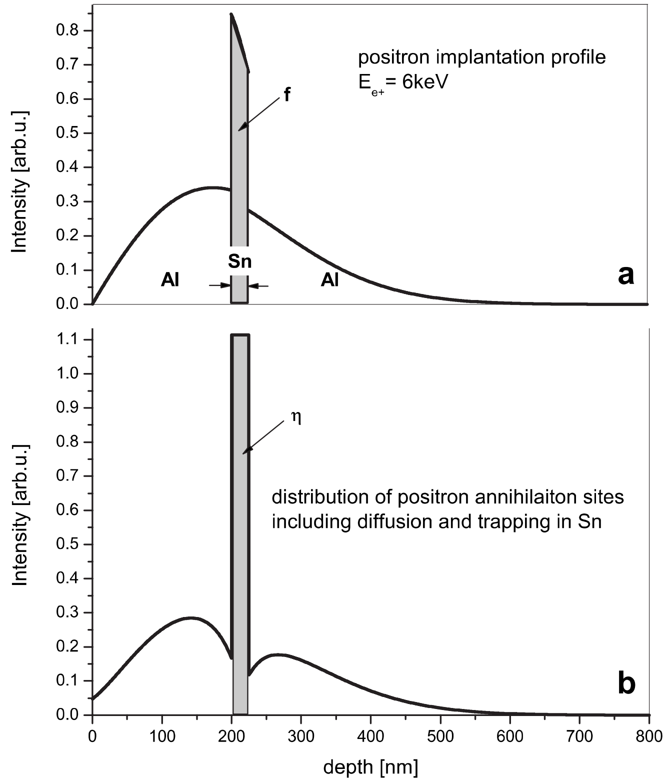

FIG. 3. (a) Implantation profile calculated for 6 keV positrons in the $Al/Sn_{25}/Al$ sample with the positron fraction f implanted in Sn (gray region). The high fraction of positrons stopped in the Sn layer reflects the high stopping power of Sn. (b) Distribution of accumulated annihilation events during diffusion and trapping in Sn. The fractions of positrons annihilating at Sn atoms η are determined from the CDB spectra.

the Al/Sn interface, where they are efficiently trapped in open-volume defects and hence could annihilate with localized core electrons of Sn atoms. A number of those defects are expected to be particularly large due to the lattice mismatch at the Al/Sn interface. On the other hand, the smaller core annihilation probability for positrons trapped in open-volume defects would lead to a lower photon intensity in the high electron momentum range than annihilation in the unperturbed Sn lattice. It is hence unlikely that defect trapping is solely responsible for the significant emergence of the Sn signature in the CDB spectra especially at low Sn thickness.

The main reason for the observed high annihilation rate in the Sn layer can be understood in terms of the element specific positron affinity: Due to the much stronger positron affinity of Sn compared to that for Al ($A^{+}_{Sn}=-7.60$ eV and $A^{+}_{Al}=-4.41$ eV),[22] the Sn layer can be regarded as a well with a potential depth of ~3.2 eV. Therefore, positrons thermalized inside the Sn layer are repelled at the Sn/Al interface during their diffusion, and a certain amount of those thermalized in Al diffuse to the Sn layer where they are efficiently trapped inside the Sn layer or Sn clusters.

The high observed annihilation rate in Sn for the sample with less than half a monolayer Sn ($d_{Sn}=0.1$ nm) leads to the interpretation that Sn (sub-)nanoparticles embedded in Al have been formed. A precondition for positron trapping inside a Sn cluster is its minimum size, i.e., the well needs a certain extension in order to possess at least one bound positron state. Supposing a spherical Sn particle, its critical radius r_c is calculated to be $r_c \cong 5.8 a_0 / \sqrt{\Delta A^+}$, where $\Delta A^+ = A^+_{\mathrm{Al}} - A^+_{\mathrm{Sn}} = 3.2$ eV is the difference of the respective positron affinities and a_0 is the Bohr radius.[22] Due to the high ΔA^+, the critical radius $r_c \cong 0.17$ nm is rather small compared to the lattice constants $a=0.65$ and 0.58 nm of the most probable Sn modifications of α-Sn and β-Sn, respectively. Therefore, even in the smallest possible cluster, a tetrahedron consisting of four Sn atoms would lead to a three-dimensional confinement of the positron in a quantum-dot-like state. This 3.2 eV deep well of Sn nanoparticles embedded in an Al matrix would act as a very efficient positron trap, which thus leads to enhanced positron trapping in the thin Sn layer.

V. CONCLUSION

Within the scope of the present work, we applied CDBS with a monoenergetic positron beam to reveal information on embedded layers with unprecedented sensitivity. It was demonstrated that even a 0.1 nm thin Sn layer embedded underneath a 200 nm Al coating leads to a significant and unambiguous fingerprint in the CDB spectrum. Besides defect trapping, we attribute the high positron affinity of Sn and the formation of Sn clusters to the most probable reason for the distinct emergence of the Sn signature for thin Sn layers. For this reason, CDBS with monoenergetic positrons is clearly a very powerful technique for the investigation of thin layered structures that are hidden below coatings of hundreds of atomic layers. We envisage to investigate layers of various elements embedded in a matrix by CDBS as a function of positron implantation energy not only to reveal the elemental information of the embedded layer but also to determine its depth below the coating.

ACKNOWLEDGMENTS

The authors thank M. Haaks from HISKP Bonn for providing the data analysis tool (MSPEC2D) for obtaining the projection from the two-dimensional CDB spectra. We gratefully acknowledge valuable discussion with P. Böni from TU Munich and with Y. Nagai from Tohoku University.

*christoph.hugenschmidt@frm2.tum.de; http://e21.frm2.tum.de/

[1] R. N. West, Adv. Phys. **22**, 263 (1973).
[2] P. J. Schulz and K. G. Lynn, Rev. Mod. Phys. **60**, 701 (1988).
[3] K. G. Lynn, J. R. MacDonald, R. A. Boie, L. C. Feldman, J. D. Gabbe, M. F. Robbins, E. Bonderup, and J. Golovchenko, Phys. Rev. Lett. **38**, 241 (1977).
[4] K. G. Lynn, J. E. Dickman, W. L. Brown, M. F. Robbins, and E. Bonderup, Phys. Rev. B **20**, 3566 (1979).
[5] P. Asoka-Kumar, M. Alatalo, V. J. Ghosh, A. C. Kruseman, B. Nielsen, and K. G. Lynn, Phys. Rev. Lett. **77**, 2097 (1996).
[6] P. E. Mijnarends, A. C. Kruseman, A. van Veen, H. Schut, and A. Bansil, J. Phys.: Condens. Matter **10**, 10383 (1998).
[7] Y. Nagai, T. Honma, Z. Tang, K. Hono, and M. Hasegawa, Philos. Mag. A **82**, 1559 (2002).
[8] M. Kostrzewa A. Baranowski, J. Beliczynski, and M. Szuszkiewicz, Nucl. Instrum. Methods Phys. Res. A **526**, 420 (2004).
[9] S. Szpala, P. Asoka-Kumar, B. Nielsen, J. P. Peng, S. Hayakawa, K. G. Lynn, and H.-J. Gossmann, Phys. Rev. B **54**, 4722 (1996).
[10] M. Alatalo, H. Kauppinen, K. Saarinen, M. J. Puska, J. Mäkinen, P. Hautojärvi, and R. M. Nieminen, Phys. Rev. B **51**, 4176 (1995).
[11] Y. Nagai, M. Hasegawa, Z. Tang, A. Hempel, K. Yubuta, T. Shimamura, Y. Kawazoe, A. Kawai, and F. Kano, Phys. Rev. B **61**, 6574 (2000).
[12] Y. Nagai, Z. Tang, M. Hassegawa, T. Kanai, and M. Saneyasu, Phys. Rev. B **63**, 134110 (2001).
[13] Z. Tang, M. Hasegawa, Y. Nagai, and M. Saito, Phys. Rev. B **65**, 195108 (2002).
[14] F. Baier and H.-E. Schaefer, Phys. Rev. B **66**, 064208 (2002).
[15] K. Sato, F. Baier, A. A. Rempel, W. Sprengel, and H.-E. Schaefer, Phys. Rev. B **68**, 214203 (2003).
[16] E. Partyka, W. Sprengel, H. Weigand, H.-E. Schaefer, F. Krogh, and G. Kostorz, Appl. Phys. Lett. **86**, 121908 (2005).
[17] Y. Takagiwa, I. Kanazawa, K. Sato, H. Murakami, Y. Kobayashi, R. Tamura, and S. Takeuchi, Phys. Rev. B **73**, 092202 (2006).
[18] M. Stadlbauer, C. Hugenschmidt, B. Straßer, and K. Schreckenbach, Appl. Surf. Sci. **252**, 3269 (2006).
[19] M. J. Puska and R. M. Nieminen, Rev. Mod. Phys. **66**, 841 (1994).
[20] C. Hugenschmidt, K. Schreckenbach, M. Stadlbauer, and B. Straßer, Nucl. Instrum. Methods Phys. Res. A **554**, 384 (2005).
[21] M. J. Koskelo, I. J. Koskelo, and B. Sielaff, Nucl. Instrum. Methods Phys. Res. A **422**, 373 (1999).
[22] M. J. Puska, P. Lanki, and R. M. Nieminen, J. Phys.: Condens. Matter **1**, 6081 (1989).